Cell Reports
Physical Science

CellPress
OPEN ACCESS

Article

Optical approaches for passive thermal management in c-Si photovoltaic modules

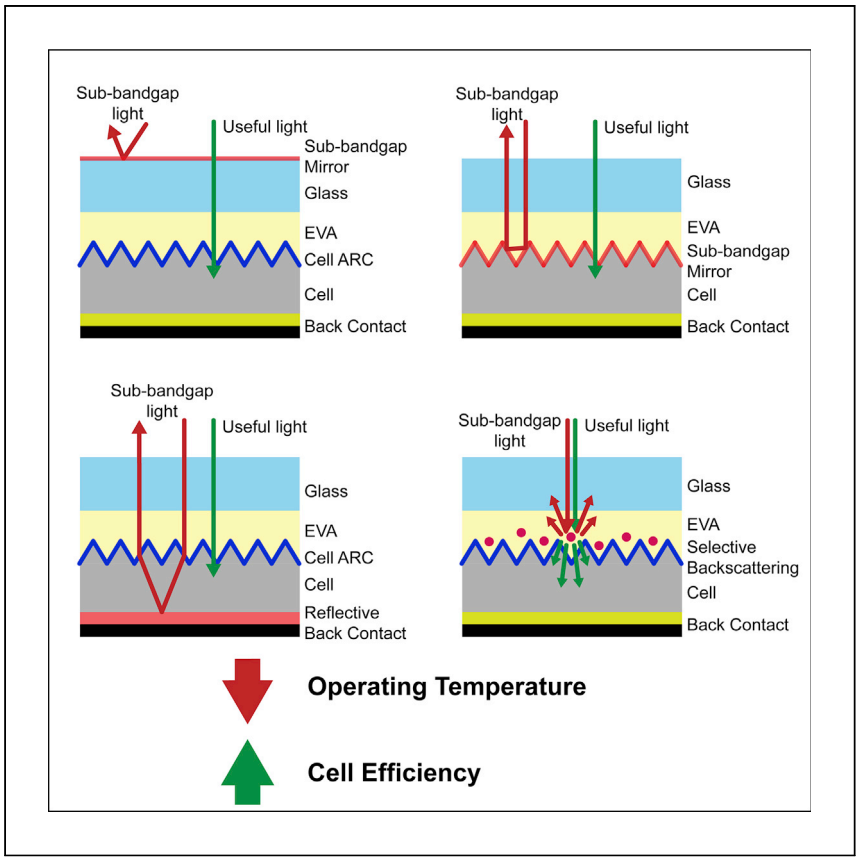

Slauch et al. provide an overview of opportunities for photovoltaic thermal management focused on the rejection of incident sub-band-gap light. They calculate reductions in waste heat generated and operating temperature via combined optical, electrical, and thermal module simulation under 1 year of realistic outdoor conditions. This method allows the determination of the limits of passive optical cooling as a function of the sub-band-gap reflectivity and the reflective interface.

Ian M. Slauch, Michael G. Deceglie, Timothy J Silverman, Vivian E. Ferry

veferry@umn.edu

Highlights

Guide for passive optical methods of cooling photovoltaic modules

Outdoor simulation of PV modules with integrated sub-band-gap reflective mirrors

Mirrors at outer glass or cell rear interface are most promising

Calculation of effects of backscattering of sub-band-gap light within the module

Slauch et al., Cell Reports Physical Science 2, 100430
May 19, 2021
https://doi.org/10.1016/j.xcrp.2021.100430

Cell Reports
Physical Science

CellPress
OPEN ACCESS

Article

Optical approaches for passive thermal management in c-Si photovoltaic modules

Ian M. Slauch,[1] Michael G. Deceglie,[2] Timothy J Silverman,[2] and Vivian E. Ferry[1,3,*]

SUMMARY

Elevated operating temperatures of solar cells encapsulated in modules lead to reduced efficiency and module lifetime. Here, we provide a comprehensive overview of the challenges and opportunities for passive optical thermal management of PV modules based on the rejection of sub-band-gap light by idealized reflectors and scatterers applied at different interfaces within crystalline Si modules and discuss the limitations to performance at each interface. We find that the annual power-weighted average operating temperature is most readily reduced via sub-band-gap reflection from the module glass, by 3.3 K for Al-BSF modules and 2.9 K for PERC modules with 100% sub-band-gap reflection. Sub-band-gap reflection at the cell interface offers up to 2.2 K (1.8 K) temperature reduction for Al-BSF (PERC) modules, increased cell rear reflection offers up to 1.2 K temperature reduction, and directional scattering offers up to 1.5 K reduction.

INTRODUCTION

Optical approaches to reduce the operating temperature of photovoltaic (PV) modules have attracted attention recently, as elevated operating temperatures both reduce the conversion efficiency by ~0.4%/K for crystalline silicon (c-Si) and decrease module lifetime.[1–3] Much of the elevated temperature derives from the parasitic absorption of sub-band-gap light. Passive strategies that focus on reducing the waste heat generated from parasitic absorption hold advantages over other strategies such as increasing radiative heat transfer from the module via high emissivity in the atmospheric transmittance window,[4] as the cooling for modules by these approaches is limited due to the already high glass emissivity.[1,5] Selective reflectors, on the outer surface of the module cover glass, are one option to reduce parasitic absorption. For example, 1-dimensional (1D) aperiodic mirrors have been designed that decrease the annual average operating temperature by ~1 K and increase the energy yield by up to 4.0% compared to a module with bare glass,[6–9] depending on the mirror design, module tilt angle, and geographic location. However, reflectors located within the module offer advantages, including protection from scratches or erosion from exposure to weathering.

While previous work has focused on model development and validation[1] and assessing and realizing specific mirror designs,[6,7,10] we focus here on assessing and comparing a variety of locations for idealized reflectors for optical passive thermal management in c-Si modules: on the front glass (Figure 1A), the textured cell front surface (Figure 1B), or the cell rear contact (Figure 1C); we also consider idealized backscatterers (Figure 1D) near the cell surface. It is essential to assess the performance of these strategies in realistic module configurations, so we compare results from aluminum back surface field (Al-BSF) modules (Figure 1E) and passivated emitter rear contact (PERC) modules (Figure 1F), in which temperature reductions are determined via combined ray-tracing

[1]Department of Chemical Engineering and Materials Science, University of Minnesota, 421 Washington Avenue SE, Minneapolis, MN 55455, USA

[2]National Renewable Energy Laboratory, Golden, CO 80401, USA

[3]Lead contact

*Correspondence: veferry@umn.edu

https://doi.org/10.1016/j.xcrp.2021.100430

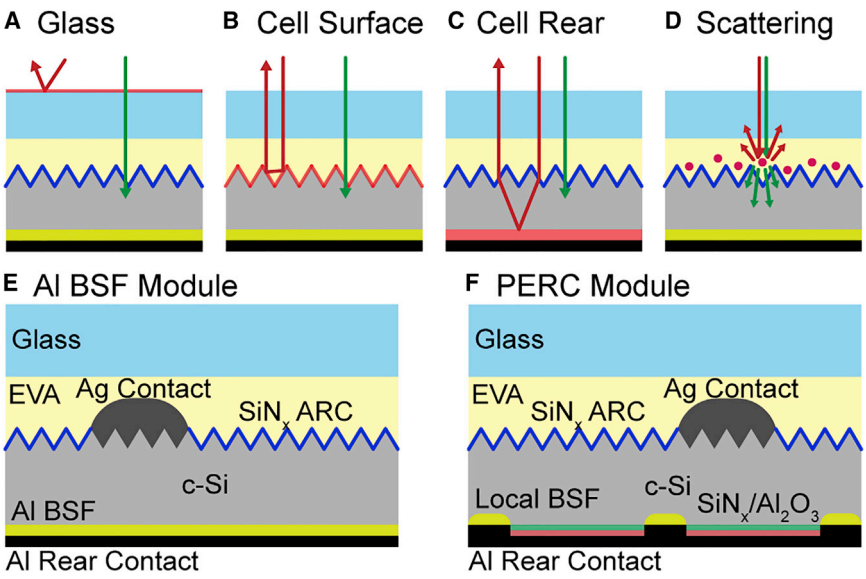

Figure 1. Thermal management concepts and module schematics

(A and B) The remaining rear area is passivated by SiN_x and Al_2O_3. We consider spectrally selective mirrors placed at (A) the outer glass and (B) the cell surface, which reflect sub-band-gap light (red arrows) and transmit above band-gap light (green arrows).

(C and D) Some simulations involve changing the (C) cell rear reflectance, which is not spectrally selective. We also consider scattering structures on the cell surface, as shown in (D).

(E and F) Schematic of the (E) Al-BSF module and the (F) PERC module used in the ray-tracing software. The Al-BSF (back surface field) module contains a full area rear BSF, while the PERC module contains local BSFs.

optical and finite element thermal and electric full-year simulations.[1] Many models exist to calculate the power or operating temperature of a photovoltaic module,[11–15] including those that consider outdoor performance[16–18] and those that consider the effects of sub-band-gap reflection.[2,4,5] Crucially, the modeling in this work accounts for time-varying irradiance, ambient temperature, wind speed, and solar position in its calculation of module temperature, while also including the influence of spectrally reflective mirrors. Therefore, this analysis establishes the limits of waste heat and operating temperature reduction for these different approaches.

This work demonstrates that spectrally selective mirrors on glass offer the greatest reductions in operating temperature. With sufficiently high reflection, spectrally selective mirrors at the cell surface can lower the module operating temperature, but multiple reflections from the cell texture limit their performance. Cell rear reflectors are the least effective at module temperature reduction; however, improvements in cell rear reflection are commonly inseparable from improvements in rear passivation quality and cell efficiency.[19–22] Provided that proper passivation is maintained, increasing cell rear reflection can provide additional thermal benefit. Finally, we show that backscattering sub-band-gap light can reduce operating temperatures as much as reflection from the cell surface; however, both approaches are limited by absorption in the glass and encapsulant.

RESULTS

Optical models for Al BSF and PERC modules agree with experimental measurements

Realistic optical models of Al-BSF and PERC modules are required to establish module reflection in the baseline case. We pay particular attention to sub-band-gap wavelengths and account for the realistic pyramidal cell texture and contact

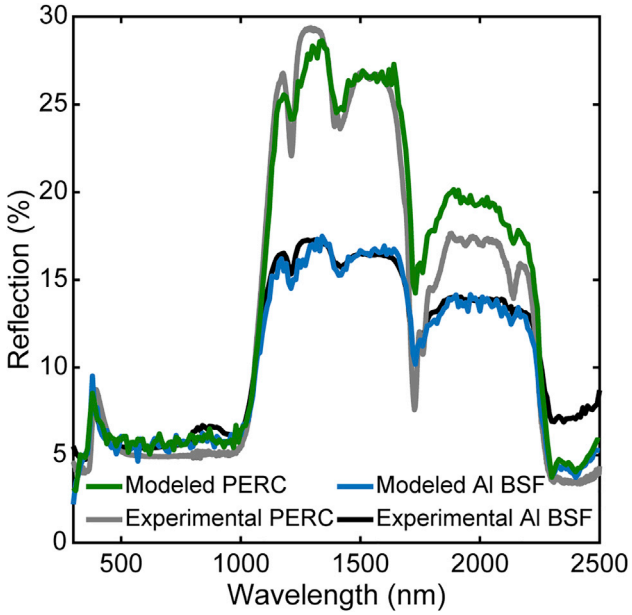

Figure 2. Modeled and experimentally measured module spectral reflection
Comparison of experimental (black/gray) and modeled (blue/green) reflection for Al-BSF and PERC modules.

roughness. Details of the ray-tracing model[23] and experimental measurements are provided in Figures S1 and S2 and Notes S1–S3. Figure 2 shows the calculated reflection alongside the experimental reflection measurements for both cases, showing good agreement across the solar spectrum.

The reflection spectra in Figure 2 can be understood in terms of the module materials and their optical properties. The low-Fe glass and ethyl vinyl acetate (EVA) encapsulant are transparent at visible wavelengths, but exhibit some sub-band-gap absorption. The EVA has absorption peaks at ~1,200, 1,400, 1,750, and 2,300–2,500 nm, which are observed in both the experimental data and the ray-tracing results. Reflection at visible wavelengths is due mostly to specular reflection from the glass, which is uncoated. A small portion of the sunlight that hits the cell surface is reflected, but between the SiN_x anti-reflection coating (ARC) on the cell surface and the pyramidal surface texturing, the vast majority is absorbed.

At sub-band-gap wavelengths, the PERC module reflects more light than the Al-BSF module. At these wavelengths, parasitic absorption occurs primarily in the cell rear contact. In the optical model for both cell types, the rear contact is Al and includes a layer of Al/Si eutectic as the back surface field, which accounts for the vast majority of the cell parasitic absorption. In the PERC cell, the back contacts are localized in a line pattern, with dielectric passivation layers between contact lines. The passivation increases the internal reflection and reduces the absorption of the PERC cell compared to Al-BSF (85% for PERC compared to 67% for Al-BSF). The external module reflection is lower than the internal reflection due to multiple reflections and light trapping within the cell.

Higher reflection from mirrors on glass compared to mirrors on the textured cell surface

Using these models as baseline cases, we incorporate idealized mirrors into Al-BSF and PERC modules at either the glass or cell surface. The idealized mirrors have

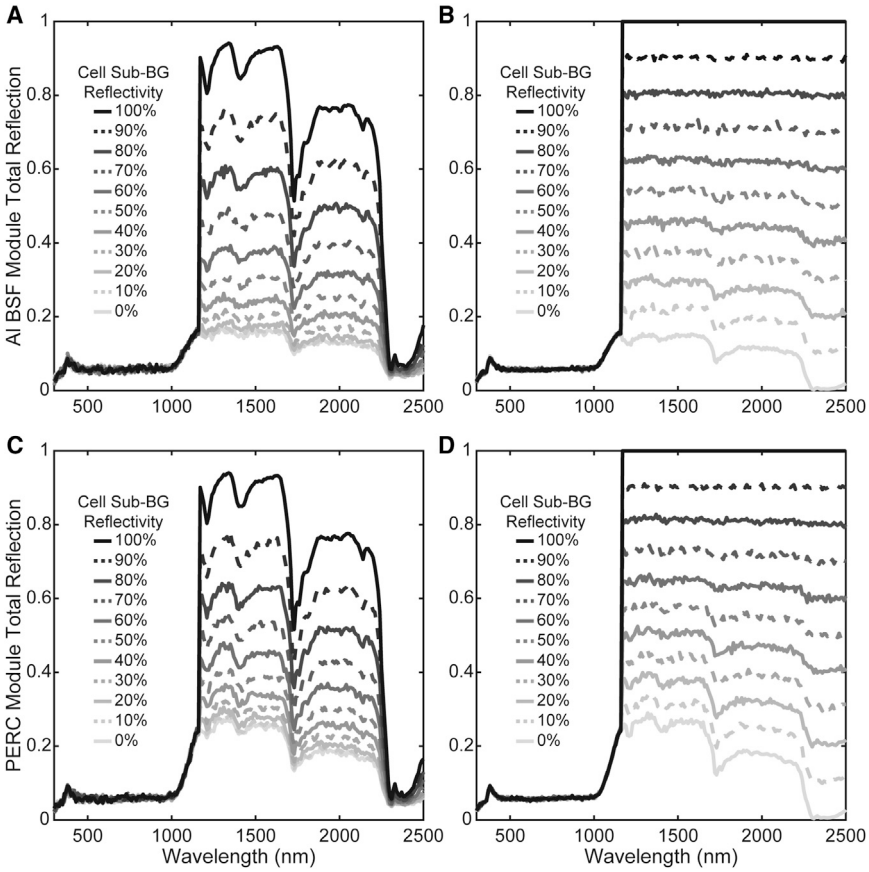

Figure 3. Sub-bandgap spectral reflection

(A–D) Module reflection for (A) and (B)—an Al BSF module and (C) and (D)—a PERC module as the sub-band-gap reflectivity of a spectrally selective mirror is varied from 0% to 100%. In (A) and (C), the mirror is on the cell surface. In (B) and (D), the mirror is on the glass. From 300 to 1,160 nm, reflection is unmodified compared to the baseline module. Incident light is normal to the module.

constant wavelength- and angle-independent reflections for $\lambda > 1{,}160$ nm, but they do not modify module reflection at shorter wavelengths, where the wavelength and angle dependence are retained. Figure 3 shows the reflection from the module at normal incidence as a function of the mirror sub-band-gap reflection for each location and each type of module. For modules with interior mirrors, module reflection is always <100%, even when the mirror reflects all sub-band-gap light, as reflection from the cell surface does not prevent parasitic absorption in the glass or encapsulant. This is particularly evident near 1,200, 1,400, 1,750, and 2,300–2,500 nm, where the encapsulant absorption is strong. Most light entering the module does not escape, even if the cell surface reflection is high. Modules that have mirrors on the outside of the glass, however, can reflect up to 100% of incident sub-band-gap light, since reflection occurs before any opportunity for parasitic absorption.

Figure 3 illustrates the limitations of designing mirrors for the cell surface. When the mirror is on the outer glass, the module reflection is at least as high as the mirror reflection since the module reflection is the sum of reflection from the mirror and reflection from the module interior. In contrast, when the mirror is applied at the cell surface, the module reflection is less than the mirror reflection. Regardless of the angle of incidence on the cell, light must reflect at least twice from the cell

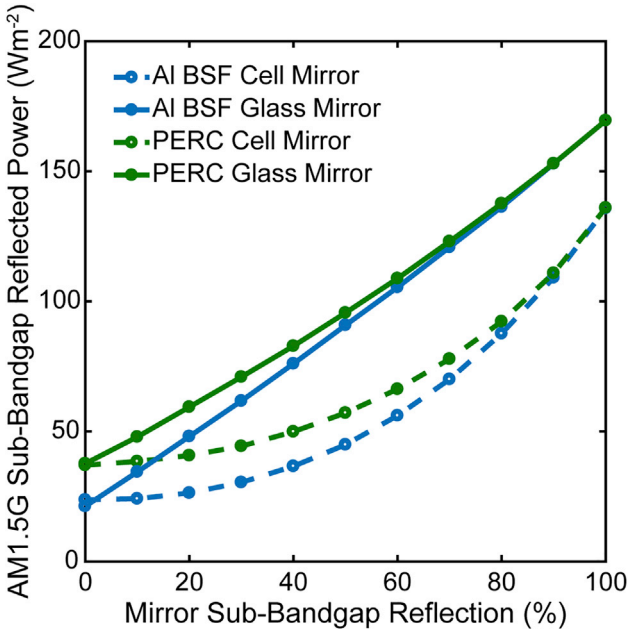

Figure 4. Sub-band-gap power reflection

Reflected power from Al BSF (blue) and PERC (green) modules as a function of idealized mirror reflection at the cell surface (dashed lines) or glass (solid lines), integrated over the sub-band-gap portion of the AM 1.5 G spectrum (>1,160 nm).

texture before escaping the module, which increases transmission to the cell.[24–26] For example, if incident light reflects twice from a 50% reflective mirror on the cell, then only 25% will return toward the module surface and 75% will transmit to the cell. This leads to a non-linear dependence of module reflection on mirror reflection at the cell surface, such that low reflectivity mirrors at this interface are ineffective.

The sub-band-gap reflected power in the AM 1.5 G spectrum is shown in Figure 4, based on the spectra in Figures 3A–3D. Modules with mirrors on the glass reflect as much as 170 Wm^{-2} sub-band-gap light, or all sub-band-gap light in the solar spectrum. Modules with mirrors on the cell reflect up to 136 Wm^{-2} sub-band-gap power. For perfectly reflective mirrors, the total power reflected by the module does not depend on the cell type since no sub-band-gap light reaches the cell. For any mirror with less than perfect reflection, the PERC module will exhibit higher reflection since the baseline PERC module reflects 37 Wm^{-2} and the baseline Al-BSF module reflects 24 Wm^{-2} sub-band-gap light. However, the mirrors provide a greater benefit to Al-BSF modules in the sense that they exhibit a greater increase in their sub-band-gap reflection.

Figure 4 also reinforces the same comparisons between glass mirrors and cell surface mirrors made above. If the mirror is applied to the cell surface, then parasitic absorption in the glass and encapsulant as well as multiple reflections from the cell texture decrease the total power reflected by the module. Even in the best-case scenario when all sub-band-gap light is reflected from the cell surface, parasitic absorption of 34 Wm^{-2}, or 20% of the incident power, cannot be prevented. The unavoidable parasitic absorption prevents cell mirrors from providing more cooling than their glass counterparts. However, in addition, both Al-BSF and PERC modules require >70% reflection at the cell surface to reject at least 85 Wm^{-2} of sub-band-gap light, or half the incident power, and >∼40% to reduce the baseline operating

temperature by >0.2 K. The multiple reflections at the cell surface place strict requirements for cooling on any mirror and are the main obstacles to sub-band-gap reflection from that interface.

Full-year outdoor simulations quantify optical advantages of mirrors on glass

We simulate idealized mirrors at the glass interface, cell interface, and cell rear under 1 full year of outdoor conditions to determine the temperature reduction achieved, making use of a previously developed combined optical, electrical, and thermal model.[1] Full-year simulations are important in the study of passive optical thermal management because they both provide realistic energy yield gain quantification and fully capture the behavior of the optics in non-normal-incidence illumination conditions outdoors. This latter point is especially important for assessing specific designs, which must effectively reflect sub-band-gap light at angles of incidence up to ~80° to be successful and have been designed elsewhere.[6–10] Simulation results also depend on the irradiance levels and wind speed at the geographic location chosen, which in this work is Denver, Colorado. In general, differences in operating temperature are magnified by low wind speed and diminished by high wind speeds, regardless of module optical properties. Further information on the simulation set up can be found in the Supplemental information, and previous efforts have estimated the impact of varying wind speed on the performance of sub-band-gap reflective mirrors.[6] In our model, module temperatures are reported relative to the baseline modules established earlier. Importantly, the operating temperature differences considered here arise only from sub-band-gap reflection, and are therefore best-case values; a realistic, optimized, mirror design for the front of the module would simultaneously reduce reflection for $\lambda < 1{,}160$ nm to some extent, as demonstrated in previous outdoor testing,[7] offering improvements in energy yield of up to 4.0%, but partially counteracting the cooling provided by sub-band-gap reflection.[4,6,10,27]

As greater sub-band-gap reflection is applied to a module, its temperature difference with respect to the baseline increases regardless of the interface at which reflection occurs. Figure 5A shows the calculated temperature differences for idealized mirrors on the glass and cell surface, and Figure 5B shows the calculated temperature differences for idealized mirrors at the cell rear. We assume that application of the idealized mirrors does not change the emissivity of the module. Annual power-weighted average temperature differences were calculated such that a positive temperature difference indicates a reduction in operating temperature. Annual average temperature reductions are significant, since their multiplication with the temperature coefficient of module efficiency gives an estimate for the percentage increase in power compared to the baseline. For all of the modules, idealized mirrors with 0% sub-band-gap reflection operate warmer than baseline modules. In the baseline modules, the glass, cell surface, and cell rear have some sub-band-gap reflection, so applying 0% reflection at either interface is a reduction in sub-band-gap reflection. In the best-case scenario, a 3.3-K annual average reduction in operating temperature was calculated for a 100% reflective mirror on glass in an Al-BSF module. Under 1 Sun conditions, the same module achieved a 6.4-K temperature reduction compared to the Al-BSF baseline.

While idealized mirrors on glass could provide >3 K annual average temperature reduction, idealized mirrors on the cell surface only offer up to 2.2 and 1.8 K annual average reduction, or 4.7 and 4.1 K reduction under 1 Sun, for Al-BSF and PERC modules, respectively. Furthermore, while the module operating temperature decreases approximately linearly with sub-band-gap reflection on glass, the

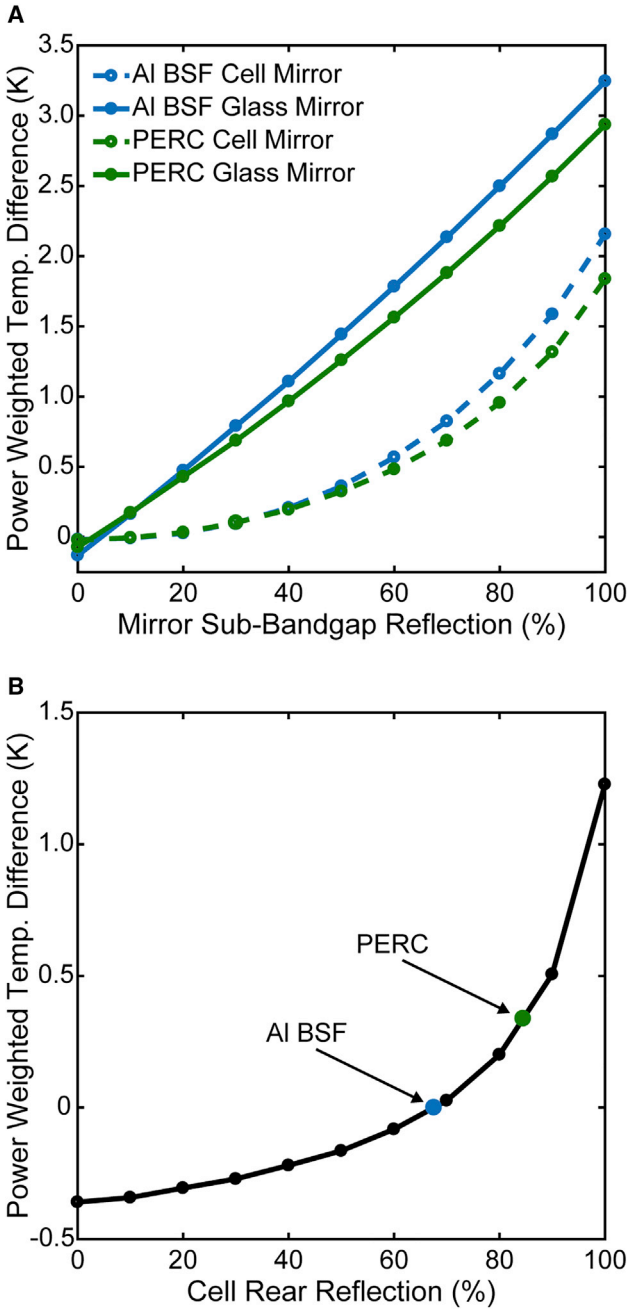

Figure 5. Operating temperature differences resulting from sub-band-gap reflection

(A) Power-weighted average module operating temperature difference from the baseline case for Al-BSF (blue) and PERC (green) modules including spectrally selective mirrors at the glass (solid lines) or cell surface (dashed lines).

(B) Temperature differences as a function of cell rear reflection (at all wavelengths). The equivalent rear reflections of Al-BSF (blue) and PERC (green) cells are marked. Temperature differences are calculated from full-year simulations, with weather and irradiance corresponding to Denver, Colorado and modules at 30° fixed tilt facing due south. Reflection was varied from 0% to 100%, shown by the circular symbols. The lines are to guide the eye.

temperature reduction has a higher-order dependence on reflection at the cell surface. As noted earlier, this indicates disadvantages for cell surface sub-band-gap reflection compared to sub-band-gap reflection from the glass. The cell texture,

which increases absorption of photons with energy above the band gap by forcing multiple reflections, also hinders the ability of spectrally selective mirrors to reduce module operating temperature, since the multiple reflections reduce light escape from the module. However, mirrors at the cell surface can still exhibit significant temperature reduction, and are protected from weathering conditions.

We also observe differences between modules containing Al-BSF and PERC cells. The data in Figure 5A show that for a given sub-band-gap reflection, the Al-BSF cells exhibit greater reduction in temperature than the PERC cells. In addition to the earlier optical results that show that the PERC module reflects more and absorbs less sub-band-gap light than the baseline Al-BSF module, the PERC cell is more efficient than the Al-BSF cell, so a greater fraction of the energy of each carrier is extracted instead of converted to waste heat. Comparison of the two baseline modules using our combined optical, thermal, and electrical simulations show the PERC module operating 0.53 K cooler than the Al-BSF module based on annual average operating temperature, or 1.05 K cooler under 1 Sun conditions. Experimentally, Vogt et al.[19] have demonstrated a 1.7-K temperature difference between PERC modules and Al-BSF modules <1,000 Wm^{-2} AM 1.5 G illumination. This larger temperature difference arises from the lack of convective heat transfer from wind. However, the temperature change relative to the baseline module is greater for Al-BSF than for PERC, as there is less waste heat generated by sub-band-gap parasitic absorption in the PERC module, and therefore less to gain by reflecting sub-band-gap light.

Temperature reduction could also be achieved by improving the reflectivity of the back contact. Unlike mirrors at the front of the cells, back contacts do not need to be spectrally selective. The PERC module is ~5% more efficient than the Al-BSF module in our simulations, an improvement arising mainly from dielectric passivation at the back contact. In the PERC cell, the Al/Si electrical contact covers a relatively small area, and the remainder is passivated by dielectrics, forming a much more reflective interface with the Al than the exposed Si. To place this in the context of the idealized mirrors discussed above, and to determine the possible temperature reductions of further improvement in back contact reflection, we include in Figure 5B points corresponding to the Al-BSF baseline (at zero temperature change) and the PERC baseline module to show the equivalent reflection of the back contact. The 0.53 K annual average temperature reduction of PERC modules compared to Al-BSF modules arises from reduced sub-band-gap absorption and improved efficiency. To determine the equivalent rear reflection of PERC cells, we run a full-year simulation using the PERC optical model, but using the Al-BSF electrical properties from Table S1. The resulting temperature difference of 0.34 K and the equivalent rear contact reflection are shown in Figure 5B. Therefore, the remaining temperature difference of 0.19 K is due to improved cell efficiency.

Overall, when varying the reflection at the back contact, the temperature reduction has a similar non-linear dependence as that seen when varying cell surface reflection. This is likely due to light trapping within the cell forcing multiple interactions of sub-band-gap light at the rear contact. While the internal reflections of the rear contact in Al-BSF and PERC modules are already high, at 67% and 85%, respectively, further temperature reduction is possible if rear contact reflection were improved.[21] However, optimizing reflection at other interfaces provides more module cooling. With 100% reflection at the rear, a 1.2-K annual average operating temperature decrease is possible, or 2.8 K under 1 Sun, although such high reflection is not realistic given the requirement to also form an electrical contact at the back surface. A 90% reflective rear surface yields only a 0.51-K annual average temperature difference, or 1.0 K under 1 Sun, compared to the Al-BSF baseline.

Spectrally selective scatterers offer the same benefit as 90% reflective cell mirrors

The existing cell surface texture forces multiple reflections of incident light and increases transmission into the cell at all wavelengths, but, as shown above, this is detrimental to the performance of mirrors on the cell surface. To circumvent this issue, we also consider an idealized application of selective backscattering to reduce the number of interactions with the cell surface. We envision scattering particles that could be embedded near the cell interface, eliminating the need to deposit multilayer reflective coatings, as shown in Figure 1D.

Highly directional scattering from spheres exhibiting both dielectric and magnetic response was first proposed by Kerker et al.[28] More recent work has demonstrated that magnetic response can be induced in dielectric particles,[29,30] and that the lowest order resonant responses, the electric and magnetic dipoles, can be tuned to enhance forward scattering.[31–36] Enhanced backscattering is possible in a properly designed dielectric nanoparticle when its electric and magnetic dipole resonances are equal in magnitude, but oscillate out of phase.[37–39] When this condition is achieved, >90% of the incident light can be backscattered after a single interaction with the particle. In our design, the scattering particle also does not interfere with or replace the existing SiN_x ARC.

A functional spectrally selective scattering nanoparticle would require a precise design, which we do not attempt in this article. Instead, we develop a model to predict the maximum temperature reduction possible in an idealized case to compare to the earlier results for mirrors. Idealized scatterers are modeled as out-of-phase electric and magnetic dipoles, and further details of our calculation method are provided in Notes S5 and S6.

The overall escape fraction, the fraction of light rejected after entering the module, as a function of wavelength for dipoles at several different distances above the cell surface are shown in Figure 6, as well as the escape fraction of the baseline module. We find that the greatest amount of light scatters and escapes the module when the scattering dipoles are placed 500 nm from the cell surface. When scattering occurs in close proximity to a substrate, phase interference between waves directly scattered toward a given direction and waves that were scattered and reflected toward that direction depends on the distance between the scatterer and the substrate. In the system of out-of-phase dipoles near the cell, the particular phase interference at a distance of 500 nm allowed more light to escape the module than any other distance investigated. In this case, either the total fraction of light backscattered was increased or a greater fraction of light was backscattered near the normal to the module surface, such that it was unlikely to be internally reflected. Placing the dipoles at distances >500 nm reduced the total amount of light escaping the module, but not by enough to increase the module operating temperature by >0.1 K compared to the 500-nm case. However, scattering too close to the substrate allows the coupling of evanescent waves above the substrate into propagating waves at oblique angles in the substrate.[40] This "forbidden light" increases the total transmission to the cell and decreases the amount of backscattering. The fraction of light escaping from the module when dipoles are placed only 100 nm from the cell surface is reduced for this reason.

When out-of-phase dipoles are placed 500 nm from the cell surface, the resulting decrease in parasitic absorption corresponds to an ~1.5-K reduction in annual module operating temperature, based on temperature reduction estimates of the model

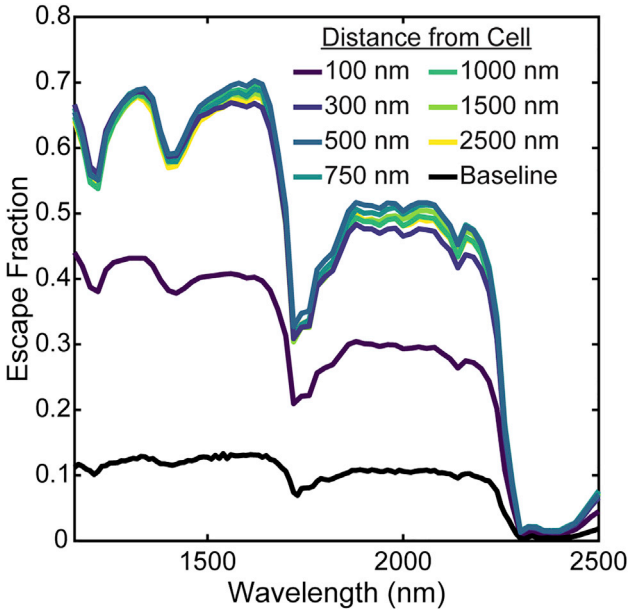

Figure 6. Sub-band-gap rejection via idealized backscattering

Escape fractions determined from the pseudo-ray-tracing algorithm for out-of-phase dipoles placed at various distances from the from the cell substrate. Once the distance reaches 300 nm, the magnitude of further changes to the escape fraction decreases. The maximum is achieved at a distance of 500 nm. For comparison, the escape fraction for the Al-BSF baseline module is also shown, determined from ray tracing.

previously used to optimize 1D mirrors.[6] The 1.5-K temperature reduction given idealized scattering is approximately equivalent to the annual average temperature reduction of a 90% reflective idealized sub-band-gap mirror at the cell surface. While it is theoretically possible to design a 100% reflective mirror, 100% backscattering particles are not possible to create, placing a bound on the effectiveness of this strategy. As is the case with spectrally selective mirrors on the cell, scattering from the cell cannot prevent absorption in the glass or encapsulant, as is evident in the minima in the escape fraction in Figure 6, which correspond to absorption peaks of those materials. Furthermore, while it is possible for a single scattering event to allow sub-band-gap light to escape the module, frequently, light is backscattered into an angle where transmission out of the module is forbidden. While one scattering event can redirect light from the cell, multiple scattering events may be required before light escapes the module. In the idealized case considered here, the vast majority of incident light will scatter backward upon any interaction, and, barring absorption into the glass or encapsulant, can be scattered backward multiple times consecutively with little probability of transmitting to the cell. However, should these idealized assumptions be relaxed, the effect of multiple scattering events, each with some probability of transmission to the cell, would likely increase parasitic absorption in a similar manner to multiple reflections from a 1D mirror.

DISCUSSION

Our simulations provide an overview of the advantages and challenges of applying the approach at different module interfaces. We show that, regardless of module type, spectrally selective mirrors on either the glass or cell surface, or increases in the cell rear reflection, can reduce the annual average module operating temperature. The largest temperature reductions are available via mirrors on the front glass of a module. These glass mirrors reflect sub-bandgap light before it enters the

module, and therefore have the greatest potential to prevent parasitic absorption. In the limit of 100% sub-band-gap reflection, cell surface mirrors cannot provide as much temperature reduction as glass mirrors, but they are protected from weathering effects inside the module. These cell interface mirrors are limited by multiple reflections from the cell texture, which allow sub-band-gap light to enter the cell unless mirror reflection approaches 100%. At the cell rear contact, improved reflection is often a side effect of modifications performed to improve the electrical properties of the cell. Even if efficiency were unchanged, our simulations show that an annual average temperature reduction up to 1.2 K is possible with increased cell rear reflection. We note that unencapsulated high-efficiency pluto cells from Suntech[22] have 65% overall sub-band-gap external reflection, a drastic improvement compared to the Al-BSF and PERC cells studied here.

Realistically, if 50%–60% sub-band-gap reflection is attained at the glass interface,[4,6,7,10] ~1.5 K temperature reductions compared to baseline are possible. Assuming a 0.39% relative increase in cell efficiency per degree,[1] ~0.6% energy yield increases are possible from the thermal effects of the mirror alone. Optimization of the mirror to provide anti-reflection of useful light could increase module energy yield further.[4,6,10,27] Anti-reflection glass coatings are becoming ubiquitous in the PV industry, but current technologies are "thermally naive" and can actually increase sub-band-gap absorption. Thermally aware glass coatings that reject sub-band-gap light while optimizing above-band-gap transmission offer a significant opportunity to increase energy yields, as we have discussed previously.[7–9]

Our results indicate that it may be possible to use scattering particles in place of a mirror at the cell surface to achieve similar performance, realizing the same benefit as a 90% reflective mirror at the cell interface. Several studies have shown directional scattering in theory and experiment,[31–39,41] but the bandwidth of the effect is small compared to the sub-band-gap portion of the solar spectrum. Zhang et al.[42] have achieved unidirectional forward scattering by a single particle in two wavelength bands, and broadband forward scattering has been demonstrated for photovoltaic applications on planar Si substrates using colloidally lithographed oligomers.[43] Techniques such as these may allow broadband backscattering in practice. Concurrent backscattering in the sub-band-gap spectral range and forward scattering visible light may require multiple particle designs, such as one set of particles tailored for backscattering sub-band-gap light and another set to forward scatter visible light. Ultimately, these scattering concepts are likely better suited to devices that operate over a narrower spectral bandwidth than the PV modules considered here.

In conclusion, we have investigated the passive temperature reduction of c-Si Al-BSF and PERC PV modules via application of spectrally selective mirrors, increases in rear contact reflection, and directional scattering. Each of these methods reduces the total parasitic absorption in a PV module by rejecting sub-band-gap light, thereby reducing the operating temperature of the module. Temperature reduction estimates follow from ray-tracing optical models, which agree with experimental module reflection measurements for both Al-BSF and PERC cells. Full-year simulations of outdoor module performance showed that the greatest reductions in operating temperatures were provided by mirrors on the outer glass, with a 100% reflective mirror offering 3.3 K temperature reduction for Al-BSF modules and 2.9 K for PERC modules for these weather conditions. Mirrors on glass reflect sub-band-gap light before it enters the module, and prevents its absorption in the encapsulant materials and the cell. Spectrally selective mirrors on the cell surface, however, cannot prevent

parasitic absorption in the glass or encapsulant. Therefore, these mirrors offer only up to 2.2 K reduction for Al-BSF and 1.8 K reduction for PERC. In addition, the textured cell surface forces multiple reflections from the mirror. When sub-band-gap reflection is <100%, as it would be in any realistic scenario, sub-band-gap transmission to the cell increases. This renders cell surface mirrors much less effective than their glass counterparts. An 80% reflective cell mirror only achieves half of the temperature reduction of a 100% reflective cell mirror, while the temperature reduction from mirrors on the front glass scales approximately linearly with mirror reflection.

Comparing simulations of Al-BSF and PERC modules, we found that the baseline PERC module operated on average 0.53 K cooler than the baseline Al-BSF module. The cooler operation of the PERC module arises from a more reflective cell rear contact and improved efficiency. Further increases to cell rear reflection could decrease the operating temperature by another 0.7 K. Spectral selectivity is not required at the cell rear, and high efficiency cells can take advantage of the high reflectivity provided by rear passivation.

Finally, we investigated spectrally selective scattering from the cell surface as a means to redirect sub-band-gap light from the module without requiring multiple interactions or multi-layer mirror deposition. We developed a method to calculate the temperature reduction from idealized scatterers, showing that a 1.5-K temperature reduction is possible, similar to a 90% reflective cell mirror. However, in terms of temperature reduction, the most effective method we have considered is spectrally selective reflection from the outer module glass.

EXPERIMENTAL PROCEDURES

Resource availability

Lead contact

Further information and requests for resources and materials should be directed to and will be fulfilled by the lead contact, Vivian Ferry (veferry@umn.edu).

Materials availability

This study did not generate new unique materials.

Data and code availability

The accession number for the data reported in this paper is UMN DRUM https://hdl.handle.net/11299/217674. Code is also available at https://github.com/NREL/pv_tomcat.

Optical, thermal, and electrical module simulation techniques

The optical properties of the baseline Al-BSF and PERC modules and all of the modules modified by spectrally selective mirrors at either the glass or cell surfaces or reflectors at the cell rear are determined from ray tracing, as described in Note S3. Thermal and electrical modeling of modules use the finite element method,[1] with the optical properties from ray tracing as inputs (Note S4). Analysis of the results determines the operating temperature and output power of each module. The differences in efficiency between Al-BSF and PERC modules are captured in this model as well.

To calculate the optical absorption in a module including directional scattering, home-written software was developed. The details are provided in Note S3.

SUPPLEMENTAL INFORMATION

Supplemental information can be found online at https://doi.org/10.1016/j.xcrp.2021.100430.

ACKNOWLEDGMENTS

The authors would like to acknowledge Dr. Greg Haugstad for performing scanning probe microscopy measurements. Part of this work was carried out with equipment supported by funding from the National Science Foundation through the UMN MRSEC under award no. DMR-2011401. This work was authored in part by the National Renewable Energy Laboratory, operated by Alliance for Sustainable Energy for the US Department of Energy (DOE) under contract no. DE-AC36-08GO28308. Funding provided by the US DOE Office of Energy Efficiency and Renewable Energy Solar Energy Technologies Office under award no. DE-EE0008542. The US Government retains and the publisher, by accepting the article for publication, acknowledges that the US Government retains a nonexclusive, paid-up, irrevocable, worldwide license to publish or reproduce the published form of this work, or allow others to do so, for US Government purposes. This report was prepared as an account of work sponsored by an agency of the US Government. Neither the US Government nor any agency thereof, nor any of their employees, makes any warranty, expressed or implied, or assumes any legal liability or responsibility for the accuracy, completeness, or usefulness of any information, apparatus, product, or process disclosed, or represents that its use would not infringe on privately owned rights. Reference herein to any specific commercial product, process, or service by trade name, trademark, manufacturer, or otherwise does not necessarily constitute or imply its endorsement, recommendation, or favoring by the US Government or any agency thereof. The views and opinions of authors expressed herein do not necessarily state or reflect those of the US Government or any agency thereof.

AUTHOR CONTRIBUTIONS

Conceptualization, I.M.S., M.G.D., T.J.S., and V.E.F.; methodology, I.M.S., M.G.D., T.J.S., and V.E.F.; investigation, I.M.S.; resources, M.G.D. and T.J.S.; writing – original draft, I.M.S., M.G.D., and V.E.F.; writing – review & editing, I.M.S., M.G.D., T.J.S., and V.E.F.; funding acquisition, M.G.D., T.J.S., and V.E.F.

DECLARATION OF INTERESTS

The authors declare no competing interests.

Received: January 9, 2021
Revised: April 7, 2021
Accepted: April 19, 2021
Published: May 19, 2021

REFERENCES

1. Silverman, T.J., Deceglie, M.G., Subedi, I., Podraza, N.J., Slauch, I.M., Ferry, V.E., and Repins, I. (2018). Reducing operating temperature in photovoltaic modules. IEEE J. Photovolt. *8*, 532–540.

2. Vaillon, R., Dupré, O., Cal, R.B., and Calaf, M. (2018). Pathways for mitigating thermal losses in solar photovoltaics. Sci. Rep. *8*, 13163.

3. McColl, S.J., Rodgers, P., and Eveloy, V. (2015). Thermal management of solar photovoltaics modules for enhanced power generation. Renew. Energy *82*, 14–20.

4. Li, W., Shi, Y., Chen, K., Zhu, L., and Fan, S. (2017). A comprehensive photonic approach for solar cell cooling. ACS Photonics *4*, 774–782.

5. Sun, X., Silverman, T.J., Zhou, Z., Khan, M.R., Bermel, P., and Alam, M.A. (2017). Optics-based approach to thermal management of photovoltaics: selective-spectral and radiative cooling. IEEE J. Photovolt. *7*, 566–574.

6. Slauch, I.M., Deceglie, M.G., Silverman, T.J., and Ferry, V.E. (2019). Model for characterization and optimization of spectrally selective structures to reduce the operating temperature and improve the energy yield of photovoltaic modules. ACS Appl. Energy Mater. *2*, 3614–3623.

7. Slauch, I.M., Deceglie, M.G., Silverman, T.J., and Ferry, V.E. (2019). Outdoor testing of c-Si photovoltaic modules with spectrally-selective mirrors for operating temperature reduction. In

Proceedings of the 46th IEEE Photovoltaic Specialists Conference.

8. Slauch, I.M., Deceglie, M.G., Silverman, T.J., and Ferry, V.E. (2018). Performance of low-complexity spectrally selective one-dimensional mirrors for photovoltaic thermal management. 2018 IEEE 7th World Conference on Photovoltaic Energy Conversion, WCPEC 2018 - A Joint Conference of 45th IEEE PVSC, 28th PVSEC and 34th EU PVSEC, pp. 2933–2938.

9. Slauch, I.M., Deceglie, M.G., Silverman, T.J., and Ferry, V.E. (2018). Two-layer anti-reflection coatings with optimized sub-bandgap reflection for solar modules. In Proceedings Volume 10759: New Concepts in Solar and Thermal Radiation Conversion and Reliability, J.N. Munday, P. Bermel, and M.D. Kempe, eds., p. 1075911.

10. Slauch, I.M., Deceglie, M.G., Silverman, T.J., and Ferry, V.E. (2018). Spectrally selective mirrors with combined optical and thermal benefit for photovoltaic module thermal management. ACS Photonics *5*, 1528–1538.

11. Mahmoud, Y., Xiao, W., and Zeineldin, H.H. (2012). A simple approach to modeling and simulation of photovoltaic modules. IEEE Trans. Sustain. Energy *3*, 185–186.

12. Aljoaba, S.Z., Cramer, A.M., and Walcott, B.L. (2013). Thermoelectrical modeling of wavelength effects on photovoltaic module performance—part I: model. IEEE J. Photovolt. *3*, 1027–1033.

13. Baenas, T., and Machado, M. (2016). Optical model for multilayer glazing systems: application to laminated glass and photovoltaic modules. Sol. Energy *125*, 256–266.

14. Hanifi, H., Pfau, C., Turek, M., and Schneider, J. (2018). A practical optical and electrical model to estimate the power losses and quantification of different heat sources in silicon based PV modules. Renew. Energy *127*, 602–612.

15. de la Parra, I., Muñoz, M., Lorenzo, E., García, M., Marcos, J., and Martínez-Moreno, F. (2017). PV performance modelling: a review in the light of quality assurance for large PV plants. Renew. Sustain. Energy Rev. *78*, 780–797.

16. Ba, M., Ramenah, H., and Tanougast, C. (2018). Forseeing energy photovoltaic output determination by a statistical model using real module temperature in the North East of France. Renew. Energy *119*, 935–948.

17. Abdolzadeh, M., and Zarei, T. (2017). Optical and thermal modeling of a photovoltaic module and experimental evaluation of the modeling performance. Environ. Prog. Sustain. Energy *36*, 277–293.

18. Duck, B.C., Fell, C.J., Anderson, K.F., Sacchetta, C., Du, Y., and Zhu, Y. (2018). Determining the value of cooling in photovoltaics for enhanced energy yield. Sol. Energy *159*, 337–345.

19. Vogt, M.R., Schulte-Huxel, H., Offer, M., Blankemeyer, S., Witteck, R., Köntges, M., Bothe, K., and Brendel, R. (2017). Reduced module operating temperature and increased yield of modules with PERC instead of Al-BSF Solar Cells. IEEE J. Photovolt. *7*, 44–50.

20. Gatz, S., Müller, J., Dullweber, T., and Brendel, R. (2012). Analysis and optimization of the bulk and rear recombination of screen-printed PERC solar cells. Energy Procedia *27*, 95–102.

21. Holman, Z.C., Filipič, M., Lipovšek, B., De Wolf, S., Smole, F., Topič, M., and Ballif, C. (2014). Parasitic absorption in the rear reflector of a silicon solar cell: simulation and measurement of the sub-bandgap reflectance for common dielectric/metal reflectors. Sol. Energy Mater. Sol. Cells *120*, 426–430.

22. Wang, Z., Han, P., Lu, H., Qian, H., Chen, L., Meng, Q., Tang, N., Gao, F., Jiang, Y., Wu, J., et al. (2012). Advanced PERC and PERL production cells with 20.3% record efficiency for standard commercial p-type silicon wafers. Prog. Photovolt. Res. Appl. *20*, 260–268.

23. SunSolve (2019). PV Lighthouse. https://www.pvlighthouse.com.au/sunsolve.

24. Baker-Finch, S.C., and McIntosh, K.R. (2011). Reflection of normally incident light from silicon solar cells with pyramidal texture. Prog. Photovolt. Res. Appl. *19*, 406–416.

25. Campbell, P., and Green, M.A. (1987). Light trapping properties of pyramidally textured surfaces. J. Appl. Physiol. *62*, 243–249.

26. Nussbaumer, H., Willeke, G., and Bucher, E. (1994). Optical behavior of textured silicon. J. Appl. Physiol. *75*, 2202–2209.

27. Zhao, B., Hu, M., Ao, X., Xuan, Q., and Pei, G. (2020). Spectrally selective approaches for passive cooling of solar cells: a review. Appl. Energy *262*, 114548.

28. Kerker, M., Wang, D.-S., and Giles, C.L. (1983). Electromagnetic scattering by magnetic spheres. J. Opt. Soc. Am. A *73*, 765–767.

29. Alù, A., and Engheta, N. (2009). The quest for magnetic plasmons at optical frequencies. Opt. Express *17*, 5723–5730.

30. Krasnok, A.E., Miroshnichenko, A.E., Belov, P.A., and Kivshar, Y.S. (2012). All-dielectric optical nanoantennas. Opt. Express *20*, 20599–20604.

31. Sikdar, D., Cheng, W., and Premaratne, M. (2015). Optically resonant magneto-electric cubic nanoantennas for ultra-directional light scattering. J. Appl. Physiol. *117*, 083101.

32. Shibanuma, T., Matsui, T., Roschuk, T., Wojcik, J., Mascher, P., Albella, P., and Maier, S.A. (2017). Experimental demonstration of tunable directional scattering of visible light from all-dielectric asymmetric dimers. ACS Photonics *4*, 489–494.

33. Albella, P., Shibanuma, T., and Maier, S.A. (2015). Switchable directional scattering of electromagnetic radiation with subwavelength asymmetric silicon dimers. Sci. Rep. *5*, 18322.

34. Luk'yanchuk, B.S., Voshchinnikov, N.V., Paniagua-Domínguez, R., and Kuznetsov, A.I. (2015). Optimum forward light scattering by spherical and spheroidal dielectric nanoparticles with high refractive index. ACS Photonics *2*, 993–999.

35. Fu, Y.H., Kuznetsov, A.I., Miroshnichenko, A.E., Yu, Y.F., and Luk'yanchuk, B. (2013). Directional visible light scattering by silicon nanoparticles. Nat. Commun. *4*, 1527.

36. Tsuchimoto, Y., Yano, T.A., Hayashi, T., and Hara, M. (2016). Fano resonant all-dielectric core/shell nanoparticles with ultrahigh scattering directionality in the visible region. Opt. Express *24*, 14451–14462.

37. Naraghi, R.R., Sukhov, S., and Dogariu, A. (2015). Directional control of scattering by all-dielectric core-shell spheres. Opt. Lett. *40*, 585–588.

38. Alaee, R., Filter, R., Lehr, D., Lederer, F., and Rockstuhl, C. (2015). A generalized Kerker condition for highly directive nanoantennas. Opt. Lett. *40*, 2645–2648.

39. Pors, A., Andersen, S.K.H., and Bozhevolnyi, S.I. (2015). Unidirectional scattering by nanoparticles near substrates: generalized Kerker conditions. Opt. Express *23*, 28808–28828.

40. Novotny, L., and Hecht, B. (2006). Principles of Nano-Optics (Cambridge University Press).

41. Geffrin, J.M., García-Cámara, B., Gómez-Medina, R., Albella, P., Froufe-Pérez, L.S., Eyraud, C., Litman, A., Vaillon, R., González, F., Nieto-Vesperinas, M., et al. (2012). Magnetic and electric coherence in forward- and back-scattered electromagnetic waves by a single dielectric subwavelength sphere. Nat. Commun. *3*, 1171.

42. Zhang, X.M., Zhang, Q., Zeng, S.J., Liu, Z.Z., and Xiao, J.-J. (2018). Dual-band unidirectional forward scattering with all-dielectric hollow nanodisk in the visible. Opt. Lett. *43*, 1275–1278.

43. Zhang, Y., Xu, Y., Chen, S., Lu, H., Chen, K., Cao, Y., Miroshnichenko, A.E., Gu, M., and Li, X. (2018). Ultra-broadband directional scattering by colloidally lithographed high-index Mie resonant oligomers and their energy-harvesting applications. ACS Appl. Mater. Interfaces *10*, 16776–16782.